Nanometer-scale molecular organization in lipid membranes studied by time-of-flight secondary ion mass spectrometry

Nanometer-scale molecular organization in lipid membranes studied by time-of-flight secondary ion mass spectrometry

Jonas K. Hannestad[a)]
RISE Research Institutes of Sweden, SE-501 15 Borås, Sweden and Department of Applied Physics, Chalmers University of Technology, SE-412 96 Göteborg, Sweden

Fredrik Höök
Department of Applied Physics, Chalmers University of Technology, SE-412 96 Göteborg, Sweden

Peter Sjövall[b)]
RISE Research Institutes of Sweden, SE-501 15 Borås, Sweden and Department of Applied Physics, Chalmers University of Technology, SE-412 96 Göteborg, Sweden

(Received 16 December 2017; accepted 24 January 2018; published 8 February 2018)

The organization of lipid membranes plays an important role in a wide range of biological processes at different length scales. Herein, the authors present a procedure based on time-of-flight secondary ion mass spectrometry (ToF-SIMS) to characterize the nanometer-scale ordering of lipids in lipid membrane structures on surfaces. While ToF-SIMS is a powerful tool for label-free analysis of lipid-containing samples, its limited spatial resolution prevents in-depth knowledge of how lipid properties affect the molecular assembly of the membrane. The authors overcome this limitation by measuring the formation of lipid dimers, originating in the same nanometer-sized primary ion impact areas. The lipid dimers reflect the local lipid environment and thus allow us to characterize the membrane miscibility on the nanometer level. Using this technique, the authors show that the chemical properties of the constituting lipids are critical for the structure and organization of the membrane on both the nanometer and micrometer length scales. Our results show that even at lipid surface compositions favoring two-phase systems, lipids are still extracted from solid, gel phase, domains into the surrounding fluid supported lipid bilayer surrounding the gel phase domains. The technique offers a means to obtain detailed knowledge of the chemical composition and organization of lipid membranes with potential application in systems where labeling is not possible, such as cell-derived supported lipid bilayers.
https://doi.org/10.1116/1.5019794

I. INTRODUCTION

Biological membranes are inherently complex, consisting of a wide range of lipids, proteins, and other constituents. Not only is the composition of the cell membrane material important, but also the spatial organization of said components. The composition of the lipid membrane is important for determining cellular function,[1] and several biological processes rely on specific local structuring of membrane components.[2,3] Additionally, several illnesses, such as Alzheimer's disease, have been linked to clustering of membrane components.[4,5] Understanding biological processes that occur within or across the cell membrane requires an understanding of the lateral organization of membrane components at different length-scales: from macroscopic structures at the micron scale down to the local molecular environment at a few nanometers. This is true also for model systems that mimic natural lipid membranes, such as supported lipid bilayers, and that consist of more than one constituent, as their applicability as model systems rely on how closely they resemble the systems that they are designed to mimic.

Here, we present a method to measure the lipid organization in supported lipid bilayers in regions as small as a few nanometers based on time-of-flight secondary ion mass spectrometry (ToF-SIMS). ToF-SIMS is a technique that is well suited for analysis of lipids, for which the detection and imaging of a wide range of molecular species with down to submicrometer spatial resolution[6] have been demonstrated, with applications covering both synthetic samples and tissues.[7–11] However, although ToF-SIMS provides a means to represent lipid surfaces in high detail, its spatial resolution is not sufficient to elucidate the finer detail of the lipid membrane composition. NanoSIMS has previously been employed to enable imaging of lipid films with nanoscale resolution.[12–15] Although NanoSIMS allows for a more fine-grained understanding of lipid membrane organization, the technique has the downside of lacking the general applicability of ToF-SIMS, as it typically requires predefined isotopic labels in order to enable unambiguous identification of analytes.

In order to test this approach for analyzing lipid films, we have devised two distinctly different scenarios: one where the two lipids are nearly chemically identical and where complete

[a)]Electronic mail: jonas.hannestad@ri.se
[b)]Electronic mail: peter.sjovall@ri.se

mixing is expected, and one where they are chemically different and where little or no mixing is expected (Fig. 1).

Our primary interest in this study is not to analyze supported lipid bilayers formed from already mixed vesicles, but rather to investigate how different lipids interact at the surface and whether they remain in isolated domains or coalesce to form homogeneous films. The formed films serve as models for how differences in chemical properties in lipid mixtures determine the molecular organization of the surface.

The different scenarios were achieved by forming lipid-coated surfaces, consisting of combinations of supported lipid bilayers and intact vesicles, using the vesicle deposition method where mixtures of two types of single component lipid vesicles (for a bicomponent lipid bilayer) were added to the silica-coated silicon substrate at a predetermined ratio. Following deposition, samples were incubated for 30 min to allow the bilayer formation (see Sec. II for further detail). After incubation, the samples were quickly frozen in liquid propane with subsequent storage in liquid nitrogen. The samples were then slowly warmed up to room temperature (RT) in vacuum (approximately 10^{-5} mbar) for solvent removal before ToF-SIMS analysis.

In the first scenario, we combine 1-palmitoyl-2-oleoyl-sn-*glycero*-3-phosphocholine (POPC) with 1-palmitoyl-2-oleoyl-sn-*glycero*-3-phosphocholine-1,1,2,2-d4-*N*,*N*,*N*-trimethyl-d9 (D13-POPC). The two lipids are chemically identical, with the exception of the isotopic labeling in the headgroup region of D13-POPC, a difference that should not impact on its capacity for blending with POPC to form a uniform supported lipid bilayer.

As a contrasting sample, we replaced POPC with 1,2-dipalmitoyl-sn-*glycero*-3-phosphocholine (DPPC). When deposited to a silica surface at room temperature, gel phase DPPC vesicles will adsorb to the surface as intact vesicles and will not collapse into a supported lipid bilayer.[16] Because of this, the extent of mixing between DPPC and D13-POPC at the surface is expected to be small. The terms

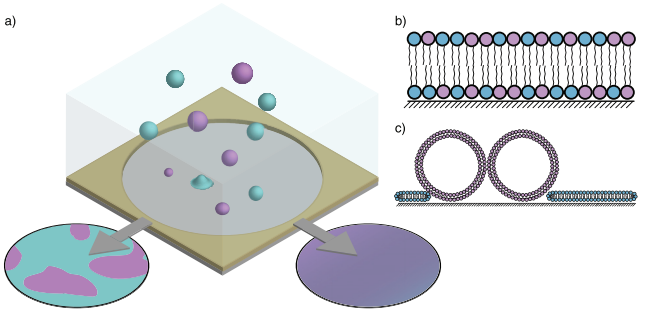

FIG. 1. (a) Schematic illustration of the formation of two-component supported lipid bilayers using the vesicle deposition method depicting two extreme scenarios with either completely isolated lipid domains (left) or full integration (right) of membrane components where the one lipid is fluid (cyan) and the other (magenta) can be either fluid or solid. Panels (b) and (c) show the expected lipid distribution on the molecular level for the mixed and isolated cases, respectively. In the extreme case of complete phase separation [depicted in (c)], the system can be characterized as a combination of planar bilayer regions and unruptured vesicles.

gel phase and fluid phase refers to the 2D mobility of the lipid molecules within the lipid bilayer under aqueous conditions, where gel phase correspond to the solid state with no mobility, whereas the lipid molecules are highly mobile and free to move within the 2D lipid membrane in the fluid phase.

To detect the abundance of the different lipid species in ToF-SIMS, one possibility is to measure the respective molecular ions. Because of the isotopic labeling of D13-POPC, we can also differentiate between the deuterated (D13-POPC) and undeuterated (POPC/DPPC) lipids by measuring peaks originating in the phosphocholine headgroup of the lipids. Furthermore, in this work, we show that the detection of molecular dimer ions can provide valuable information about the molecular organization at the nanometer level, as previously demonstrated for distinguishing between crystalline and amorphous phases in pharmaceutical compounds.[17] Figure 2(a) shows an example mass spectrum in positive polarity for a mixed sample containing D13-POPC and DPPC with molecular, dimer, and headgroup fragment ions for both the deuterated and nondeuterated lipids indicated in the spectrum. Figure 2(b) shows the molecular structure of the different phospholipids used in this study. The different mass peaks in positive polarity and their respective assignments are presented in Table I.

II. MATERIALS AND METHODS

A. Lipids

POPC, D13-POPC, and DPPC were purchased from Avanti Polar Lipids dissolved in chloroform and used without further purification or as powder and later dissolved in methanol. Phosphate buffered saline (PBS), used as buffer in the experiments, was purchased from Sigma-Aldrich.

B. Liposome preparation

The lipid material, dissolved in either chloroform or methanol, was evaporated at the bottom of a round flask under a gentle stream of N_2. Residual solvent was removed by exposing the interiors of the flask with the dried lipid film to vacuum for a minimum of 1 h. The film was then hydrated with 1 ml of PBS buffer and vortexed until a turbid whitish liquid was obtained (approximately 5 min). The lipid suspension was then extruded 11 times through a 100 nm polycarbonate membrane (Whatman, UK) using a mini extruder (Avanti Polar Lipids, Inc.) resulting in a clear vesicle solution with a total lipid concentration of 2 mg/ml. Rehydration of the lipid film and subsequent extrusion was performed at room temperature for POPC and D13-POPC and at 42 °C for DPPC.

C. Time of flight-secondary ion mass spectrometry

Samples for ToF-SIMS analysis were prepared by depositing lipid vesicles onto Si-wafers coated with a 60 μm thick layer of SU-8 with a 3 mm in diameter large hole, acting as a sample chamber (the substrate design is previously described

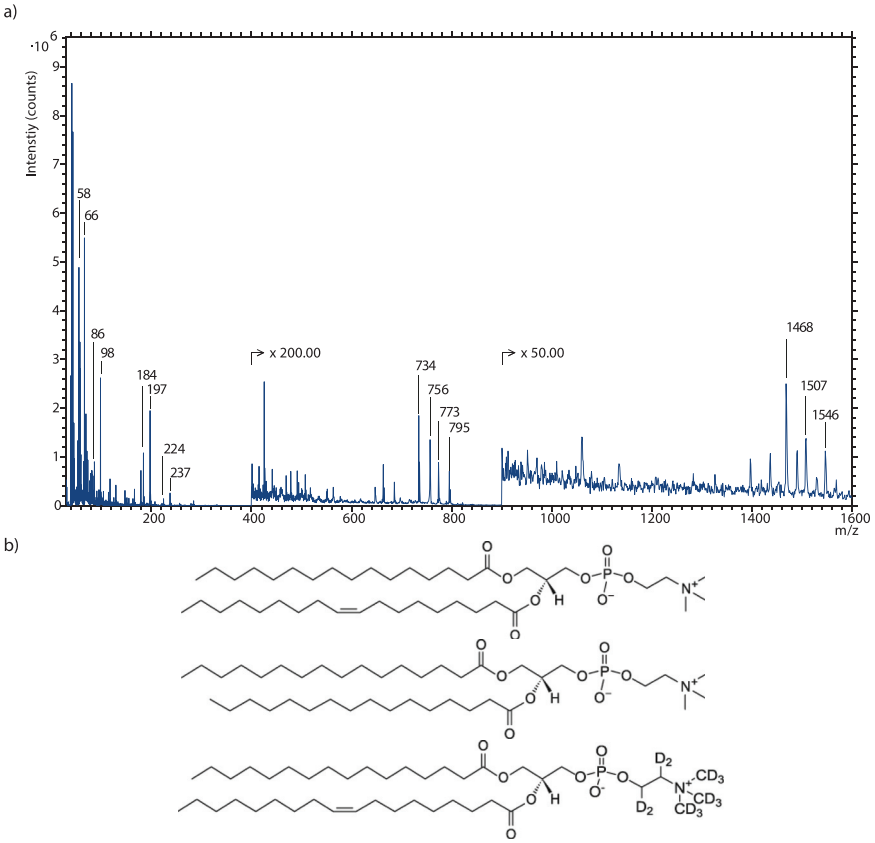

FIG. 2. (a) Example spectrum for a phospholipid film containing a mixture of DPPC and D13-POPC. Numbers in the spectrum indicate the mass peaks for headgroup fragments, molecular and dimer ions. The intensity in the mass spectrum is multiplied by factor 200 at *m*/*z* 400 and again by factor 50 at *m*/*z* 900 to allow visualization of a wider range of mass peaks. (b) Molecular structure of POPC, DPPC, and D13-POPC (top to bottom).

by Sjövall *et al.*[18]). 100 μl lipid vesicle solutions, at total lipid concentration 0.1 mg/ml in PBS, were added to the sample chamber and incubated at RT for 30 min. During incubation, the samples were kept in closed containers to avoid excessive buffer evaporation. Halfway through the incubation, the samples were mixed by pipetting a fraction of the solution up and down a few times.

Following incubation, samples were rinsed, first with PBS to remove unbound material, and then followed by three subsequent washing steps in ultrapure water to remove salts. After rinsing, water was carefully removed from the substrates leaving a thin liquid film covering the sample area. The samples were then quickly frozen in liquid propane and kept in liquid nitrogen until being placed in vacuum overnight to remove the water.

Analysis of the lipid samples was performed in a TOFSIMS IV instrument (IONTOF GmbH) using 25 keV Bi_3^+ primary ions. The instrument was utilized with settings favoring either high mass or high spatial resolution. At high mass resolution, the mass resolving power is in the order of 3000–8000 (m/Δm) and the spatial resolution is in the range between 3 and 5 μm, while the spatial resolution is roughly 200–400 nm with nominal mass resolution (m/Δm ∼ 300) in the high spatial resolution mode. The maximum primary ion dose density was 5.0×10^{11} and 2.3×10^{12} for high mass and high spatial resolution modes, respectively. For measurements at high mass resolution, a 500×500 μm^2 surface was imaged using 256×256 pixel resolution, while the imaged area was 50×50 μm^2, divided over 512×512 pixels, for the high spatial resolution measurements.

III. RESULTS AND DISCUSSION

In order to capture different compositional states of the hybrid supported lipid bilayers, we analyzed samples from a broad range of mixing ratios. The overall composition of the lipid membrane was primarily evaluated using the relative intensities of the different headgroup fragments, determined through the peak areas measured in high mass resolution mode. Further, images obtained in high spatial resolution mode show whether the different lipids are present at the surface either in a uniform lipid film with complete miscibility, or in two phase systems with discrete single-lipid domains. This dual evaluation process provides a good measure of the overall quality of the lipid bilayer allowing both quantification of the relative abundance of the different phospholipid species in the surface as well as giving an estimate of their spatial distribution across the surface from the obtained peak intensity images.

Figure 3 shows the results from the first scenario where POPC and D13-POPC is mixed. Figure 3(a) shows example mass spectra for 100%, 50%, and 0% D13-POPC in the lipid vesicle mixture used to form the bilayer, showing the

TABLE I. Mass units and peak assignments for deuterated and undeuterated phosphocholine headgroup fragments together with molecular ions for DPPC, POPC, and D13-POPC as well as dimer ions from possible combinations of the same phospholipids.

Phosphocholine headgroup fragment ions in positive polarity			
Undeuterated		Deuterated	
Mass (*m*/*z*)	Assignment	Mass (*m*/*z*)	Assignment
58.07	C_3H_8N	66.11	C_3D_8N
86.11	$C_5H_{12}N$	98.18	$C_5D_{12}N$
104.12	$C_5H_{14}NO$	117.19	$C_5D_{13}HNO$
166.09	$C_5H_{13}PO_3$	179.19	$C_5D_{13}NPO_3$
184.11	$C_5H_{15}NO_4P$	197.19	$C_5D_{13}H_2NO_4P$
224.14	$C_8H_{19}NO_4P$	237.20	$C_8D_{13}H_6NO_4P$
Molecular and dimer ions			
Mass (*m*/*z*)		Assignment	
734.59		M+H (DPPC)	
756.45		M+Na (DPPC)	
760.66		M+H (POPC)	
773.68		M+H (D13-POPC)	
795.54		M+Na (D13-POPC)	
1468.19		2M+H (DPPC+DPPC)	
1507.26		2M+H (DPPC+D13-POPC)	
1520.32		2M+H (POPC+POPC)	
1533.34		2M+H (POPC+D13-POPC)	
1546.37		2M+H (D13-POPC+D13-POPC)	

molecular ion for the two molecular species. The results show a clear trend where the peak intensity follows linearly the fraction of the corresponding species in the lipid mixture. At the 50% point, the abundance for POPC and D13-POPC is equal. We observe the same trend for the phosphocholine headgroup fragments, presented in Fig. 3(b) as an average of the intensities for the different fragment ions over a range of mixing ratios. The figure indicates a linear dependence in the surface abundance on the sample composition, where the relative abundance of, e.g., POPC in the surface follows directly from the fraction of POPC in the added vesicle mixture.

The results above are also reflected in the imaged surfaces where we observe the same trend of decreasing ion intensity with decreasing sample fraction. High-resolution images of the added intensities of deuterated and undeuterated phosphocholine headgroup fragments can be seen in Fig. 3(c) for 100%, 50%, and 0% D13-POPC. The images show that the lipid material is evenly distributed across the entire surface and that there are only minor regions with noticeable deviation from the average intensity for either lipid species. This indicates that the combination of POPC and D13-POPC form a homogeneous supported lipid bilayer, irrespective of the ratio between the two lipids, which is the expected result.

It is worth noting that of all the different fragment ions selected to represent the abundance of the corresponding lipids, $C_5H_{15}NO_4P^+$ and its deuterated counterpart constitute something of a special case, since the formation of this specific fragment ion requires the addition of a hydrogen atom/ion from the molecular surroundings. In the samples mixing deuterated and nondeuterated POPC, this "external" hydrogen can be either a proton or a deuteron and, consequently, this specific fragment ion splits into two peaks in the spectrum. The intensity distribution between the two fragments, $C_5D_{13}H_2NO_4P^+$ and $C_5D_{14}HNO_4P^+$, with nominal masses 197 and 198, respectively, (presented as a function of D13-POPC fraction in Fig. S1, supplementary material[28]), thus provides information about the molecular mixing in the mixed bilayer and about the fraction of external hydrogens that come from neighboring head groups (i.e., D) and from the fatty acid tails (i.e., H) in the pure D13-POPC bilayer.

The second scenario, where D13-POPC is instead combined with DPPC, presents a more complex behavior, as can be seen from the results presented in Fig. 4. The molecular ion intensities of DPPC (M + H *m*/*z* 734.59) and D13-POPC (M + H *m*/*z* 773.68) are shown for DPPC ratios 0.25, 0.55, and 0.95. Similarly to the previous case, we observe a trend where the abundance of one specific lipid species increases with its fraction in the added vesicle mixture. Figure 4(b) shows the average relative abundance of deuterated and undeuterated phosphocoholine headgroup fragment ions, respectively, as a function of the DPPC fraction in the added vesicle mixture. Here, the results are markedly different compared to the previous case. There is a noticeable "lag" phase where the DPPC content in the surface (as indicated by the abundance of undeuterated headgroup fragments) only marginally increases with increasing DPPC fraction in the vesicle mixture, followed by a sharp increase in DPPC surface content at higher fractions.

This difference in abundance can be explained through the difference in how the different lipid species behave when their respective vesicles adsorb to the silica substrate. Given that a vesicle adsorbs to a surface at all, it will follow one of three different pathways: it can either rupture right away to form a bilayer on the surface; it can remain intact until a critical surface coverage is reached before it ruptures and forms a bilayer; or it can remain intact throughout and not form a bilayer at all.[19] Here, DPPC vesicles will remain intact when they land at the surface, whereas POPC vesicles will initially be found at the surface until a critical coverage is reached, which will cause the vesicles to rupture and form a bilayer in an avalanchelike fashion.

When the supported lipid bilayer forms, the surface area covered by each incorporated POPC vesicle will increase by a factor of 4 (surface area of a sphere versus projected area on the surface), thereby quickly covering any still free surface area and preventing new vesicles to be adsorbed. At low DPPC fraction, the critical coverage for POPC bilayer formation will be reached quickly, giving little opportunity for intact DPPC vesicles to bind to the surface, hence the low DPPC abundance observed. In contrast, at high DPPC fraction, accumulation of sufficient amounts of POPC vesicles takes longer time, allowing more DPPC vesicles to bind. In addition, the presence of intact DPPC vesicles at the

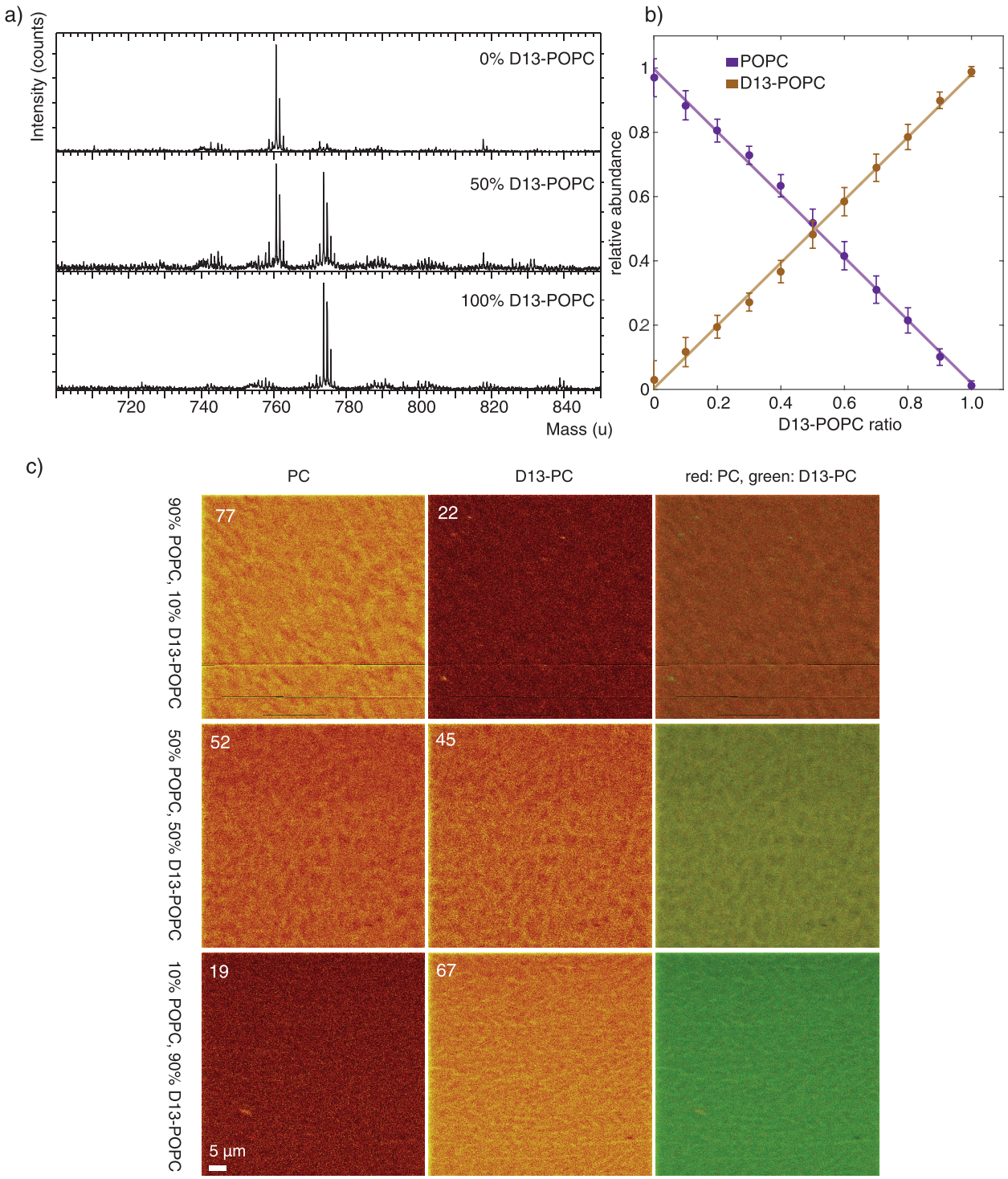

FIG. 3. (a) Example spectra in positive polarity showing the molecular ion peaks for POPC (M+H m/z 760.66) and D13-POPC (M+H m/z 773.68) for POPC fractions 0, 0.5, and 1 in the added vesicle mixture. (b) Average relative surface abundance of deuterated (m/z 66.11, 98.18, 117.19, 179.19, 197.19, and 237.20) and undeuterated (m/z 58.07, 86.11, 104.12, 166.09, 184.11, and 224.14) phosphocholine headgroups as a function of D13-POPC fraction in the sample. Linear fits to the data show that the measured ion abundances matches what is expected from the lipid mixing ratio of the sample and also serve as a guide to the eye. (c) High-resolution images of the deuterated (D13-PC) and undeuterated (PC) phosphocholine headgroup fragments at different POPC fractions, presented separately and overlaid with the deuterated fragments colored red and the undeuterated fragments colored green (right column). The image brightness indicates intensity (counts), increasing linearly to the maximum value indicated by the figure in the top left corner for each ion image. Pixel size $125 \times 125\,\text{nm}^2$.

surface further hinders bilayer formation by acting as obstacles to the lipid film propagation, thereby allowing even more DPPC vesicles being adsorbed. This escalation in DPPC coverage can be seen in the graph in Fig. 4(b) which shows only marginal increases in relative abundance of DPPC associated ion with increasing DPPC concentration at low DPPC ratios, followed by a steep increase in relative DPPC abundance at approximately 0.6 DPPC.

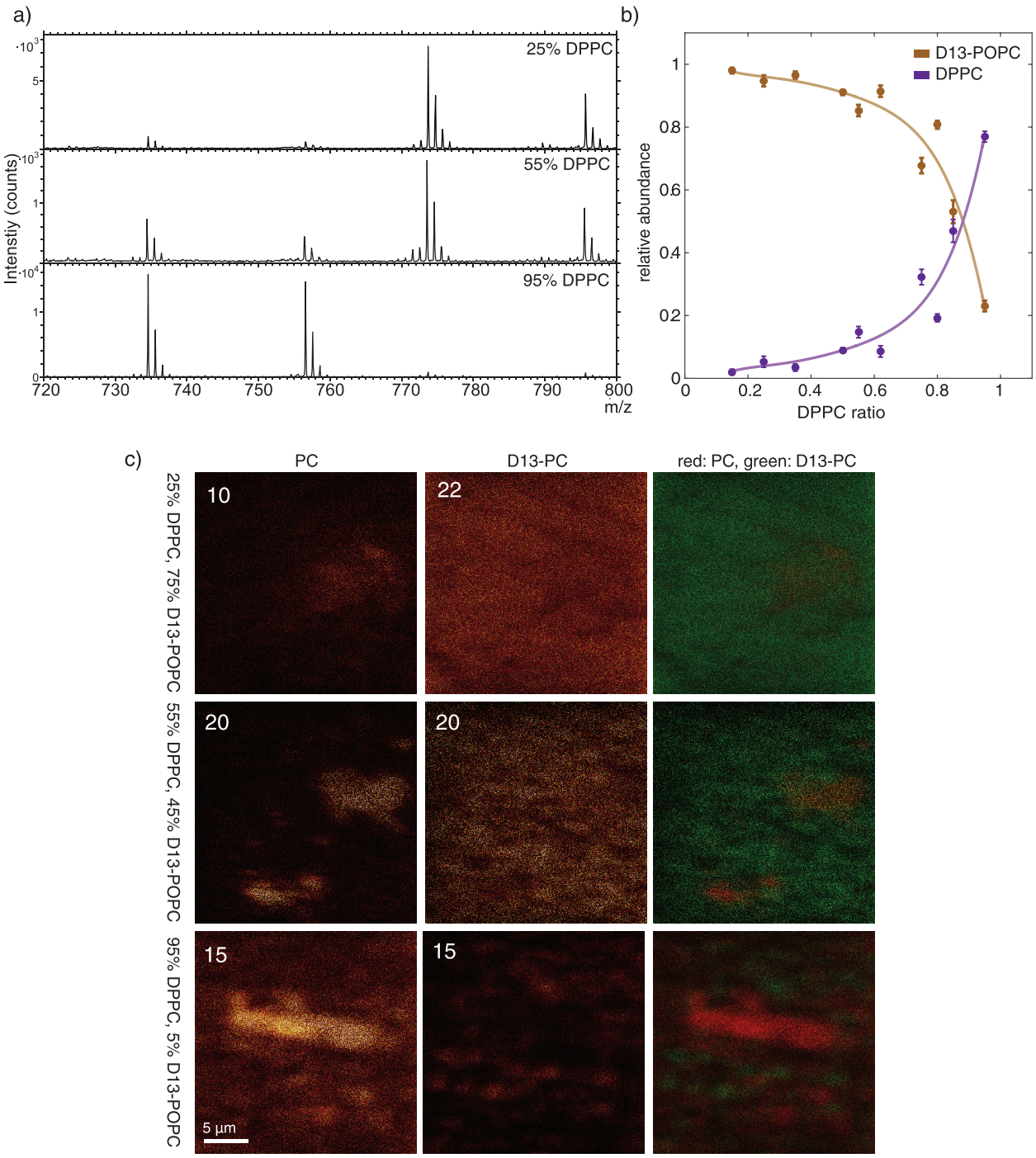

FIG. 4. (a) Example spectra in positive polarity showing the molecular ion peaks for DPPC (M + H *m*/*z* 760.66) and D13-POPC (M + H *m*/*z* 773.68) for DPPC fraction x, x, and x. (b) Average relative surface abundance of deuterated (*m*/*z* 66.11, 98.18, 117.19, 179.19, 197.19, and 237.20) and undeuterated (*m*/*z* 58.07, 86.11, 104.12, 166.09, 184.11, and 224.14) phosphocholine headgroups as a function of DPPC fraction in the added vesicle mixture. Polynomial fits to the data serves as a guide to the eye. (c) High-resolution images of the deuterated (D13-PC) and undeuterated (PC) phosphocholine headgroup fragments at different DPPC fractions, presented separately and overlaid with the undeuterated fragments colored red and the deuterated fragments colored green (right column). The image brightness indicates intensity, increasing linearly to the maximum value indicated by the figure in the top left corner for each ion image. Pixel size $98 \times 98\,\mathrm{nm}^2$.

Compared to the combination of POPC and D13-POPC, we see a much more pronounced abundance of sodium adducts (M+Na), for the 95% DPPC sample, in particular, as can be seen in the spectra in Fig. 4(a). This might be due to the presence of intact DPPC vesicles that maintain their interior buffer solution throughout the washing steps, which would result in higher sodium content at the surface when all solvent is evaporated as the samples are exposed to vacuum.

The high spatial resolution images paint a drastically different picture compared to the fully homogeneous

POPC/D13-POPC supported lipid bilayers. Figure 4(c) presents example images of the lipid surface at 0.25, 0.55, and 0.95 DPPC fractions. The overall ion intensity trend in the images follows the same pattern as was presented for the quantification of PC headgroup abundance in Fig. 4(b). At DPPC ratios below 0.25, the intensity for undeuterated PC headgroup fragments is very low, which is why we present that level as the lowest DPPC fraction. In contrast to the previous example, the organization of material at the surface changes greatly with changes in the level of DPPC content. At 25% DPPC, the surface is dominated by D13-POPC, which is spread out over the entire surface with individual patches of DPPC. It should be noted that although DPPC is confined to isolated regions, those regions do not exclude D13-POPC. This indicates that within these regions there are planar domains consisting of a mixture of DPPC and D13-POPC. While this behavior is maintained when the DPPC level increases, smaller, more defined, patches start to appear together with an increase in the overall intensity across the entire surface. This shows that DPPC does not integrate in the surface in one single way, but rather covers a range of mixing conditions, including complete integration, diffuse regions of higher concentration to distinct single content domains. This complex distribution of content is indicative of the phase behavior of lipid bilayer consisting of mixtures of DPPC and POPC at room temperature, where the overall lipid membrane is in a regime of coexistence between liquid and gel phase that extends up to roughly 90% DPPC. The increased DPPC content in the surface is reflected in the D13-POPC distribution which, while still covering the entire imaged surface, appears patchier than what was the case for the homogenous distribution at lower DPPC ratios. The properties of the surface also change with increasing DPPC content. Analysis of the surface characteristics using quartz crystal microbalance with dissipation monitoring (QCM-D), presented in Fig. S2, shows decreasing bilayer formation with increasing DPPC concentration. However, limited bilayer formation is observed as high as 90% DPPC.

At 95% DPPC, the surface is dominated by gel phase lipid with POPC only being present in isolated spots that appear spatially separated from the DPPC-covered regions. DPPC, on the other hand, is both present as an overall surface-covering film and in dense, material rich, oblong structures [see, e.g., the bright region in Fig. 4(c), bottom row]. Similar structures found in POPC/DPPC hybrid vesicles have previously been reported by Shoemaker and Kyle Vanderlick.[20]

While the combination of quantification of lipid membrane content and high resolution surface imaging provides a clear picture of the differences in overall membrane organization and characteristics between hybrid supported lipid bilayers consisting of POPC and D13-POPC, and DPPC and D13-POPC, the results still do not reflect the local microenvironment experienced by the individual membrane components. To obtain this level of detail, which is of great importance for the understanding of the behavior of membrane and membrane associated components, we need more fine-grained measures of membrane composition and organization.

In ToF-SIMS, the detected secondary ions are produced by bombardment of the sample surface with a stream of primary ions, where each individual ion impact releases enough energy to eject from the surface a large number of molecular fragments and intact molecules, of which a small fraction is ionized and can thus be registered in the time-of-flight detector. The primary ion impact, which results in an impact crater of roughly 5 nm in diameter, can also generate new molecular bonds, such as the dimerization of lipid molecules in the lipid membrane.[21] This dimerization process can be utilized to gain information of the nanometer-scale molecular organization on the sample surface, since, in order to form a dimer, the two molecules that comprise it need to be present within the same 5 nm diameter patch. This means that by measuring the dimer ions from the sample, we get an estimate of the composition of the surface on the level of a few nm. In this particular case, the presence of lipid dimers—which can be either homodimers made up of two identical lipid molecules or heterodimers, which consist of two lipid molecules that are different—will be an indicator of the nanometer mixing of the surface in the analyzed part of the sample.

In our setup, the two-component lipid mixture gives rise to three different possible dimers, two homodimers and one heterodimer, each. The specific dimers and their associated masses can be found in Table I. Figures 5(a) and 5(b) show the detected dimers for the hybrid supported lipid bilayers at different mixing ratios containing POPC/D13-POPC and DPPC/D13-POPC, respectively. Both cases show a similar trend where the two homodimers dominate in separate ends of the mixing spectrum and where the abundance of the respective heterodimer increases.

The results presented in Figs. 5(b) and 5(d) show that for both types of phospholipid hybrid films, the formation of heterodimers as a function of surface composition follows a parabolic shape, culminating where the ratio between the two constituents is 1:1 on the surface. Note that the relative abundances in Figs. 5(b) and 5(d) are plotted versus the measured D13-POPC and DPPC ratios on the lipid surfaces, respectively, and not versus mixing ratio of the vesicle solution used to form the bilayer (as was shown in Figs. 3 and 4). This change does not greatly affect the results for the POPC/D13-POPC mixture, since the composition of the surface closely resembles the bulk lipid proportions. However, for DPPC/D13-POPC, the heterodimer peak in Fig. 5(d) is shifted toward lower DPPC ratios compared to the equivalent plot against the bulk fraction of DPPC.

To determine the degree of mixing in the analyzed lipid films, we have devised an expression, presented in Eq. (1), for how the abundance of homo- and heterodimers depend on the relative concentrations of the lipid monomers for a completely mixed bilayer, as well as on a mixing fraction variable, r, which describes the deviation from perfect mixing, e.g., due to isolated monoconstituent domains on the surface,

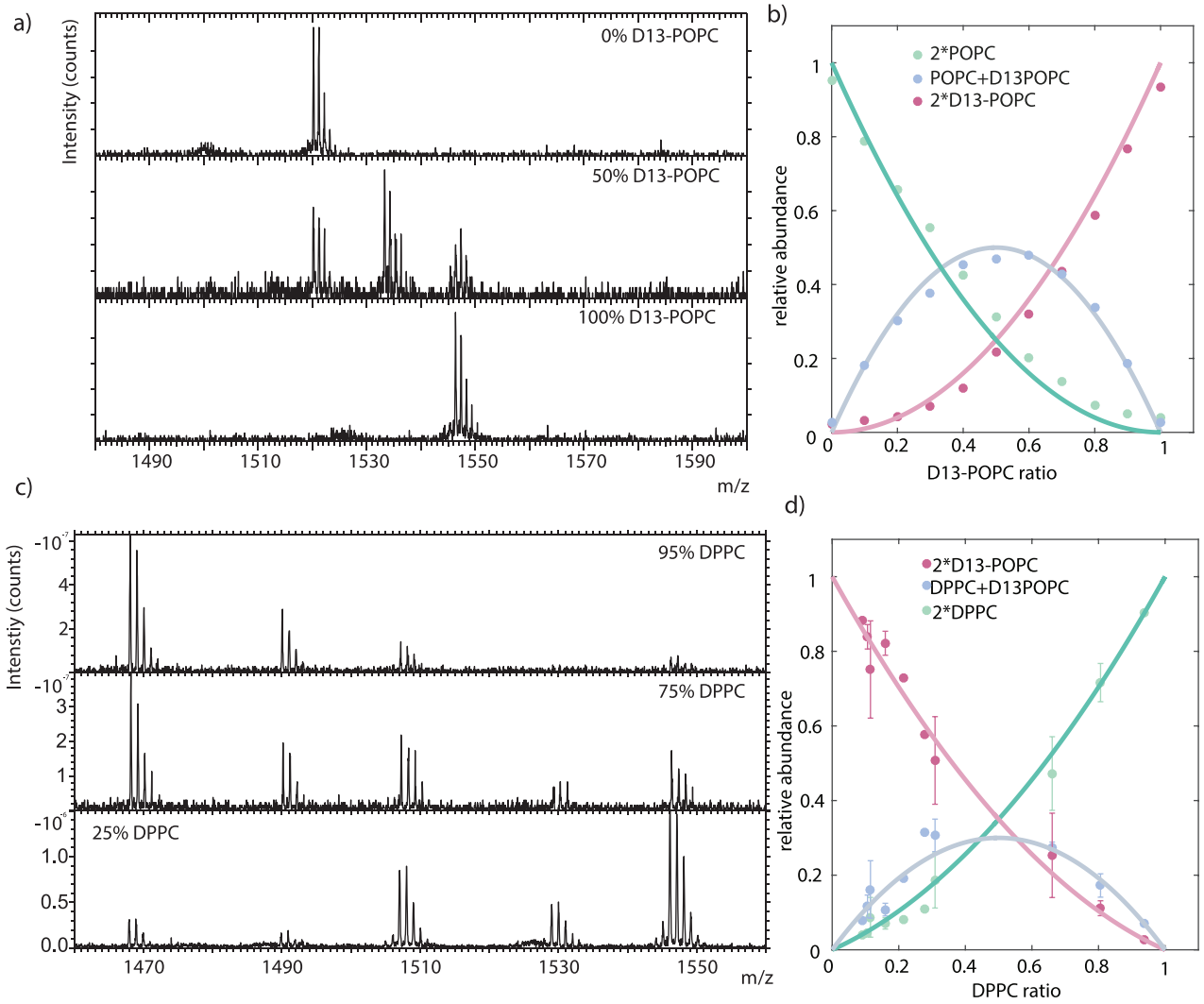

FIG. 5. (a) Example spectra of POPC/D13-POPC dimers for 0%, 50%, and 100% D13-POPC. The spectra show $(POPC)_2$ and $(D13\text{-}POPC)_2$ homodimers (m/z 1520.32 and 1546.37, respectively), as well as (POPC)(D13-POPC) heterodimer (m/z 1533.34). Each spectrum is normalized to the highest peak intensity. (b) Relative abundance of $(POPC)_2$ (green), (POPC)(D13-POPC) (blue), and $(D13\text{-}POPC)_2$ (red) dimers as a function of the measured D13-POPC fraction in the sample. Line plots constitutes fits of the measured data to the expressions in Eq. (1) (*vide infra*) with r = 1. (c) Example spectra of DPPC/D13-POPC dimers for 25%, 55%, and 95% DPPC. The spectra show DPPC+DPPC and D13-POPC+D13-POPC homodimers (m/z 1468.19 and 1546.37, respectively), as well as DPPC+D13-POPC heterodimer (m/z 1507.26). (d) Relative abundance of $(DPPC)_2$ (green), (DPPC)(D13-POPC) (blue), and $(D13\text{-}POPC)_2$ (red) dimers as a function of the measured DPPC fraction in the sample. Line plots constitutes fits of the measured data to the expressions in Eq. (1) (*vide infra*) with r = 0.6.

$$AA = (1-r)A + rA^2, \tag{1a}$$

$$BB = (1-r)(1-A) + r(1-A)^2, \tag{1b}$$

$$AB = 1 - (AA + BB), \tag{1c}$$

$$AB = 2r(A - A^2). \tag{1d}$$

The expressions in Eqs. (1a)–(1c), where A and B are the relative concentrations of the specific monomers (and $B = 1 - A$), AA, BB the two homodimers, AB the heterodimer, and r the mixing fraction, result in the expression for the heterodimer abundance in Eq. (1d), which is plotted in Figs. 6(a) and 6(b) as a function of monomer fraction for different values for r. Doing this provides a possibility space where lipid membranes with varying composition and content organization will occupy different regions of the plotted area. In Figs. 6(a) and 6(b), we have added the experimentally determined heterodimer relative abundances at different monomer ratios for the combinations of POPC/D13-POPC and DPPC/D13-POPC, respectively, (black circles). Here, we see that, for the POPC/D13-POPC lipid film, the detected heterodimer abundance lies close to the top of the parabolic space, corresponding to complete mixing ($r = 1$), whereas DPPC/D13-POPC is positioned more centrally. Fitting the experimental data to the heterodimer curves for different values of r gives us an estimate of the degree of mixing in the membranes for different monomer compositions, presented for both discussed cases in Fig. 6(c). Here, we see that the combination of POPC/D13-POPC results in a supported lipid bilayer with complete content mixing, irrespective of the relative concentration of said contents, which is the expected result since there is no chemical reason for the two lipid species to not mix. The

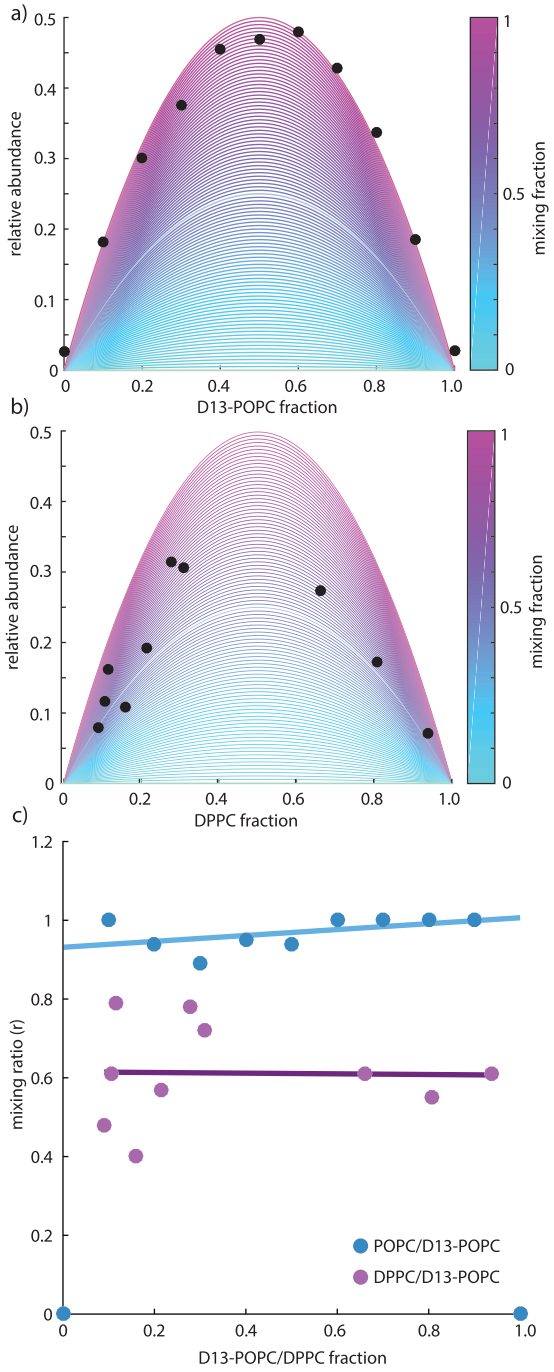

FIG. 6. (a) Measured relative abundance of (POPC)(D13-POPC) heterodimer (black dots) shown together with calculated possible heterodimer abundances for different degree of mixing and different D13-POPC fractions determined according to Eq. (1). (b) Measured relative abundance of (DPPC)(D13-POPC) heterodimer (black dots) shown together with calculated possible heterodimer abundances for different degree of mixing and different DPPC fractions determined according to Eq. (1). (c) Mixing ratio fit of the experimentally determined relative abundances for (POPC)(D13-POPC) (blue) and (DPPC)(D13-POPC) (cyan) heterodimers to the mixing ratio model in Eq. (1). The plotted data is fitted with a linear expression (blue and cyan lines).

DPPC/D13-POPC hybrid lipid film, on the other hand, has an overall mixing fraction of 0.6. This value for the mixing fraction shows that many of the DPPC molecules in the surface are incorporated into a DPPC/POPC hybrid film, although they are deposited as purely DPPC vesicles. At low DPPC ratios, DPPC and POPC are able to fully blend with each other forming a homogeneous fluid phase.[20,22] According to the DPPC/POPC phase diagram, the transition between a single fluid phase and a coexisting two-phase system containing one fluid and one gel phase occurs at room temperature at roughly 35% DPPC.[20,22] The overall characterization of the membrane composition obtained from the PC headgroup fragment abundances show that this transition ratio in the membrane is reached at approximately 70% added DPPC. This means for many of the analyzed DPPC/D13-POPC hybrid surfaces, we would expect to see complete mixing of the two lipid species. The fact that we do not observe complete mixing indicates that some of the DPPC in the membrane maintain its gel phase characteristics and does not transition into the overall lipid membrane. This is consistent with our result [presented in Fig. 4(c)] showing distinct DPPC domains even at lower ratios. Further, the decrease in content mixing at increasing DPPC concentration is also reflected in the QCM-D results (presented in Fig. S2) which show decreasing bilayer formation with increasing DPPC content on the sensor surface. This likely affects both DPPC, which in itself is prone to partition into isolated domains, and POPC alike. When large parts of the surface are covered by solid domains dominated by DPPC, these domains will also prevent the formation of POPC supported lipid bilayers as well.

When extending the DPPC concentration in the membrane above the partitioning of the lipid mixture into two coexisting phases, the lipid dimer results show that we still maintain a high level of mixing between the DPPC and D13-POPC membrane content. This shows that, although a complete integration of the two materials is not possible, a large amount of DPPC still blends with D13-POPC in the surface. This again is consistent with the images of the overall organization of the membrane at high DPPC ratios showing a very complex composition containing a surface-covering lipid film, small domains and large, elongated and dense clusters. The integration of DPPC into the fluid phase of the lipid film has previously been observed. Åkesson *et al.* report a decrease in liquid phase mobility at high DPPC fraction, detected using fluorescence recovery after photobleaching.[23] Similarly, Burns *et al.* report, using fluorescence correlation spectroscopy, differential mobility in different parts of the hybrid lipid surface.[24] Of particular interest is the decreased mobility of the fluid phase in the regions close to DPPC patches, pointing toward the formation of areas where DPPC is incorporated from the isolated patches into the POPC supported lipid bilayer.

IV. SUMMARY AND CONCLUSIONS

We have in this work shown that ToF-SIMS can be used to obtain wide-range characterization of heterogeneous supported lipid bilayers providing a micrometer scale perspective on the overall structure and organization of the lipid surface and at the same time offering information about the

local microenvironment of the membrane constituents on the nanometer scale through the detection of lipid dimers produced in individual primary ion impact events.

Our results show that hybrid lipid systems with differing properties have vastly different content organization from the formation of micron-scale domains to the distribution of lipid molecules on the nanometer scale. While the combination of the chemically identical lipids POPC and D13-POPC results in a miscible supported lipid, from the individual molecules in the long-range structure of the membrane, the contrasting example of DPPC and D13-POPC provides a much more complex picture of membrane organization.

The combination of DPPC and D13-POPC results in a range of different structures at varying lipid ratios, including extended fluid lipid bilayers, isolated smaller domains with limited content overlap between the two membrane constituents and dense oblong single-lipid gel phase structures. The last structure type is almost exclusively present at higher DPPC concentrations, reflecting the separation into a two-phase system at a high fraction of gel-phase lipids as well as the presence of unruptured DPPC vesicles on the surface. Whereas the molecular mixing in the POPC/D13-POPC bilayer occurs at the theoretical maximum at all investigated lipid ratios, the blending efficiency of DPPC and D13-POPC is 60% of what is statistically possible. The extent of mixing is interesting, in particular at high DPPC ratios, showing that even when DPPC partitions into distinct gel phase domains, fractions of the DPPC can be extracted into the fluid phase of the D13-POPC bilayer.

We have in this work used isotopically labeled lipids. However, it is not a choice born out of necessity and is nothing that prevents the utilization of the technique where such labeling is not possible. Rather, it serves to set up an extreme point by allowing comparison of two chemically identical lipids that still allow separation in the obtained mass spectrum. Instead, it is systems where labeling options do not exist and where other high-resolution techniques such as NanoSIMS are not viable, or where chemical information resolving power of NanoSIMS is desired, where this technique provides the most new opportunities.

By obtaining knowledge on the molecular scale about the constitution of supported lipid bilayers, we can increase the surface content complexity when using supported lipid bilayers as model systems for biological membranes while still retaining in-depth knowledge about the constitution of the model system. This becomes even more relevant where experimental membrane models are made more similar to the biological systems they mimic through the incorporation of cell-derived lipid membranes.[25–27] While this makes the lipid system function better as biological model systems, it also removes direct control over the molecular composition of the vesicular composition. Importantly, our approach allows elucidation of the molecular constitution of lipid membrane systems in great detail. This result is great value in the study of complex, biologically relevant, membrane system where knowledge of the lipid composition is limited.

ACKNOWLEDGMENTS

This work was supported by the Swedish Research Council (Contract No. 2015-04199). The authors would also like to acknowledge Björn Agnarsson for supplying the microsctrutured SU-8 coated silicon chips.

[1]A. A. Spector and M. A. Yorek, J. Lipid Res. **26**, 1015 (1985), available at http://www.jlr.org/content/26/9/1015.
[2]K. Simons and D. Toomre, Nat. Rev. Mol. Cell Biol. **1**, 31 (2000).
[3]D. Lingwood and K. Simons, Science **327**, 46 (2010).
[4]K. Matsuzaki, Acc. Chem. Res. **47**, 2397 (2014).
[5]G. Di Paolo and T. W. Kim, Nat. Rev. Neurosci. **12**, 284 (2011).
[6]C. Prinz, F. Höök, J. Malm, and P. Sjövall, Langmuir **23**, 8035 (2007).
[7]A. Brunelle, D. Touboul, and O. Laprevote, J. Mass Spectrom. **40**, 985 (2005).
[8]K. Chughtai and R. M. A. Heeren, Chem. Rev. **110**, 3237 (2010).
[9]L. Carlred *et al*., J. Am. Chem. Soc. **136**, 9973 (2014).
[10]S. Sole-Domenech *et al*., Acta Neuropathol. **125**, 145 (2013).
[11]A. Gunnarsson, F. Kollmer, S. Sohn, F. Höök, and P. Sjövall, Anal. Chem. **82**, 2426 (2010).
[12]C. Galli Marxer, M. L. Kraft, P. K. Weber, I. D. Hutcheon, and S. G. Boxer, Biophys. J. **88**, 2965 (2005).
[13]M. L. Kraft, P. K. Weber, M. L. Longo, I. D. Hutcheon, and S. G. Boxer, Science **313**, 1948 (2006).
[14]M. M. Lozano, Z. Liu, E. Sunnick, A. Janshoff, K. Kumar, and S. G. Boxer, J. Am. Chem. Soc. **135**, 5620 (2013).
[15]M. M. Lozano, J. S. Hovis, F. R. Moss, and S. G. Boxer, J. Am. Chem. Soc. **138**, 9996 (2016).
[16]Z. Wang and S. Yang, Langmuir **24**, 11616 (2008).
[17]A. Iuraş, D. J. Scurr, C. Boissier, M. L. Nicholas, C. J. Roberts, and M. R. Alexander, Anal. Chem. **88**, 3481 (2016).
[18]P. Sjövall, B. Agnarsson, L. Carlred, A. Gunnarsson, and F. Höök, Surf. Interface Anal. **46**, 707 (2014).
[19]R. P. Richter, R. Bérat, and A. R. Brisson, Langmuir **22**, 3497 (2006).
[20]S. D. Shoemaker and T. Kyle Vanderlick, Biophys. J. **84**, 998 (2003).
[21]V. Thiel and P. Sjovall, *Principles and Practice of Analytical Techniques in Geosciences* (The Royal Society of Chemistry, London, 2015), p 122.
[22]W. Curatolo, B. Sears, and L. J. Neuringer, Biochim. Biophys. Acta **817**, 261 (1985).
[23]A. Åkesson, T. Lind, N. Ehrlich, D. Stamou, H. Wacklin, and M. Cardenas, Soft Matter **8**, 5658 (2012).
[24]A. R. Burns, D. J. Frankel, and T. Buranda, Biophys. J. **89**, 1081 (2005).
[25]H. Pace, L. Simonsson Nyström, A. Gunnarsson, E. Eck, C. Monson, S. Geschwindner, A. Snijder, and F. Höök, Anal. Chem. **87**, 9194 (2015).
[26]O. Wahlsten, A. Gunnarsson, L. Simonsson Nyström, H. Pace, S. Geschwindner, and F. Höök, Langmuir **31**, 10774 (2015).
[27]M. J. Richards, C.-Y. Hsia, R. R. Singh, H. Haider, J. Kumpf, T. Kawate, and S. Daniel, Langmuir **32**, 2963 (2016).
[28]See supplementary material at https://doi.org/10.1116/1.5019794 for ToF-SIMS analysis of $C_5H_{15}NO_4P+$ abundance and QCM-D analysis of supported bilayer formation for different POPC/DPPC vesicle mixtures.